

Article

Adsorption Characteristics of Phenolic Compounds on Graphene Oxide and Reduced Graphene Oxide: A Batch Experiment Combined Theory Calculation

Xiaobo Wang^{1,2,†}, Yanhui Hu^{1,†}, Jianhua Min¹, Sijie Li¹, Xiangyi Deng¹, Songdong Yuan^{3,*} and Xiaohua Zuo^{1,*}

¹ College of Chemistry and Chemical Engineering, Hubei Polytechnic University, Huangshi 435003, China; wangxb@hust.edu.cn (X.W.); 211044@hbpu.edu.cn (Y.H.); jianhuaminmin@163.com (J.M.); 13995970512@163.com (S.L.); dengxiangyi2018@163.com (X.D.)

² College of Chemistry and Chemical Engineering, Huazhong University of Science and Technology, Wuhan 430074, China

³ Hubei Collaborative Innovation Center for High-efficiency Utilization of Solar Energy, Hubei University of Technology, Wuhan 430068, China

* Correspondence: yuansd2001@163.com (S.Y.); zuoxiaohua111@163.com (X.Z.); Tel.: +86-027-59750870 (S.Y.); +86-0714-6357654 (X.Z.)

† These authors contributed equally to this work.

Received: 15 September 2018; Accepted: 6 October 2018; Published: 17 October 2018



Abstract: A series of phenolic compounds containing 2-phenylphenol (PPE), bisphenol A (BPA), 4-isopropylphenol (IPE), 4-methylphenol (ME) and phenol (PE) were selected to investigate their major influence factors for their adsorption on graphene oxide (GO) and reduced graphene oxide (RGO) by studying their adsorption isotherms and kinetics. It was found that the adsorption of all tested phenols fitted well with the Freundlich model. In comparison, the adsorption ability of RGO with a stronger π - π interaction was superior to GO, which was confirmed by using naphthalene probe measurements. The thermodynamic characteristics, by studying the effect of the adsorption temperatures (298, 313 and 333 K), demonstrated that the adsorption process was spontaneous, exothermic and entropy-decreasing. The chemical structures of the phenols also affected their adsorption on GO and RGO. It was found that the adsorption capacities of phenols were, in order, PE (0.271 mmol g⁻¹ on GO and 0.483 mmol g⁻¹ on RGO) < ME (0.356 and 0.841 mmol g⁻¹) < IPE (0.454 and 1.117 mmol g⁻¹) < BPA (0.4 and 1.56 mmol g⁻¹) < PPE (0.7 and 2.054 mmol g⁻¹), which depended on the π -electron density of the benzene ring by means of a density functional theory (DFT) calculation. Undoubtedly, the reduction of GO and an increase in π -electron density on the chemical structures of phenols facilitated the adsorption.

Keywords: reduced graphene oxide; π - π interaction; phenolic compounds; adsorption

1. Introduction

Phenolic compounds with high toxicity are considered to be representative of undesirable pollutants and have become a focus point of environmental study. Phenolic pollution trends have been rising for at least the past 10 years because of discharge of waste water from paints, pesticides, polymeric resin, petroleum and so on [1]. A large number of studies have focused on waste water purification contaminated by phenols, and various techniques have been developed to efficiently remove them. At present, the most widely used methods for phenol removal have included biological degradation [2,3], photocatalytic decomposition [4,5], chemical oxidation [6,7],

hydrodynamic cavitation [8,9] and adsorption [10–13]. Among these approaches, adsorption seem to have a particular advantage due to its relatively low cost, speed and convenience of operation.

Graphene is a new two-dimensional surface carbon material formed by the composition of an sp^2 hybrid orbital with a single carbon atom sheet structure and has aroused great interest since the report of Novoselov et al. [14]. Graphene promised to be an excellent adsorbent due to its huge specific surface area and excellent adsorption performances, with a high adsorption capacity and fast adsorption rate. For example, Zhou et al. [15] studied the adsorption behaviors of ten halogenated aliphatic compounds on a graphene nanosheet and demonstrated that hydrophobic and π - π electron donor-acceptor interactions were the adsorption mechanisms. Majidi et al. [16] made use of density functional theory to calculate the adsorption of caffeine and nicotine molecules on graphene sheets, indicating high adsorption energies for both. Xu et al. [17] summarized the graphene-based nanomaterials used for the adsorption of heavy metal ions. The functionalized bare derivatives of graphene-based nanomaterials exhibited better adsorption performance and a higher adsorptive capacity for aqueous heavy metals removal. As an oxidative product of graphite and a precursor for graphene preparation, graphene oxide (GO) was decorated with various oxygen-containing groups with a very high negative charge density such as hydroxyl, epoxy and carboxyl groups. The extremely hydrophilic nature and specific surface structure make GO able to purify waste water as an adsorbent. For example, Yang et al. [18] systematically investigated the adsorption of trivalent antimony (Sb(III)) on GO. It was found that GO had a strong adsorption ability for Sb(III) within a wide pH range of 2.0 to 10.0. Ramesha et al. [19] revealed that GO could efficiently remove cationic dyes.

In recent decades, a great deal of work has focused on the adsorption process of aromatic compounds. Among them, the concept of π - π stacking was widely accepted to describe the face-to-face stacking of aromatic systems involved in noncovalent interactions [20–22]. It should be noted that graphene is more suitable for the adsorption of aromatic compounds with a benzene ring. Numerous experimental studies indicated that graphene had relatively higher sorption capacities and a stronger sorption affinity for aromatic compounds than nonaromatics [13,23]. Most of the research only explored the phenomenon description, rather than the exact sorption mechanism. On the basis of several theoretical calculation studies, it was believed that the π - π interactions between aromatic adsorbates and graphene played the most important role, which depended on the electron density of the aromatic system and the adsorbate structure [24–26]. However, these theoretical studies were only limited to a small portion of the benzene-ring units of graphene. In addition, very few experimental studies systematically investigated the interactions between π -acceptor or donor aromatics and graphene. Therefore, it was necessary to combine detailed experimental and theoretical calculation studies for the description of the adsorption mechanism.

The goal of the current research was to reveal the adsorption characteristics of aromatics for graphene. To this end, five kinds of phenolic compounds were selected and the adsorption characteristics of them on reduced graphene oxide (RGO) and GO with a different π -electron density as adsorbents were studied. The effect of the molecular structure of adsorbates on the adsorptive interaction was also investigated. In order to further verify the research viewpoints, the electron distribution of phenols was also investigated by theoretical calculation. We anticipate that this study could fill the knowledge gap of the underlying sorption mechanism of aromatics on RGO and GO.

2. Experimental Procedure

2.1. Materials

Graphite powder (SP1 graphite) was purchased from American Bay Carbon (Bay City, MI, USA). 2-phenylphenol (PPE), bisphenol A (BPA), 4-isopropylphenol (IPE), phenol (PE), 4-methylphenol (ME) and other chemicals were obtained from China Sinopharm Group. All the chemicals were of analytical grade.

2.2. Preparation of RGO

A modified Hummers method was used for the preparation of GO (see Supplementary Materials for more details). RGO was synthesized by a chemical reduction method. Generally, 100 mL GO aqueous dispersion (0.2 g) was added into three flasks, placed in an oil bath pan at 95 °C 0.2 g hydrazine hydrate (80 wt.%), and was dropwise added and reacted for 5 h while stirring. After that, the mixture was centrifuged and washed with deionized water sequentially. At the end, the solid was redispersed in water as RGO dispersions.

2.3. Characterization

X-ray photoelectron spectroscopic (XPS) analysis was observed on a VG Multilab 2000 spectrometer. A Malvern Zetasizer Nano-ZS90 was used to measure zeta potentials. The surface morphology was characterized on a Hitachi S-4800 scanning electron microscope (SEM). The Raman spectrum was measured on a Thermo Fisher DXR equipped with a charge-coupled device (CCD) detector. Fourier transform infrared (FT-IR) spectra were measured on a Bruker VERTEX 70.

2.4. Batch Adsorption Experiments

A certain amount of the phenol solutions was separately added to sealed conical flasks and then positioned on a shaker at 180 rpm. The solution volume was made up to 45 mL by water, and the typical pH of the solution was adjusted to 7. After that, 3 mg GO or RGO aqueous dispersion (5 mL) was added into the solution. The initial concentration of GO or RGO was 60 mg L⁻¹. The initial concentration ranges of PE, ME, IPE, BPA and PPE were 0.053–0.85, 0.046–0.55, 0.073–0.587, 0.087–0.35 and 0.059–0.47 mmol L⁻¹, respectively. Solutions were sampled at regular intervals and centrifuged to remove the solids. The phenol concentration in the supernatant was determined on a UV-Vis spectrophotometer (CARY 50Scan). The adsorbed amount of phenols at equilibrium was calculated with Equation (1),

$$q_e = \frac{(c_0 - c_e)V}{m} \quad (1)$$

where q_e (mmol g⁻¹) is the equilibrium adsorption capacity of the adsorbent, c_0 and c_e (mmol L⁻¹) are the initial and final concentrations of the phenols in solution, V is the solution volume, and m is the mass of the used GO and RGO. The adsorption kinetic experiment times included 1, 5, 10, 15, 30, and 60 min. The adsorption thermodynamics temperatures included 298, 313 and 333 K and the pH range for the effect on adsorption was 3–11.5. Generally, the typical experiments were performed in duplicate/triplicate.

3. Results and Discussion

3.1. Characterization of GO and RGO

The surface morphology of GO and RGO was investigated by SEM characterization. As seen from the results (Figure 1), the samples were composed of corrugated ripple-like sheets, which showed the substantive characteristics of graphene. The surface oxygen functional groups of GO made it seemed as if the crumpled sheets were stuck together. After the GO was reduced, the topographic characteristics of RGO evolved into an analogous mass of dark clouds, and the wrinkled sheets were increased and randomly aggregated to a certain degree, which led to the formation of well-developed mesopores.

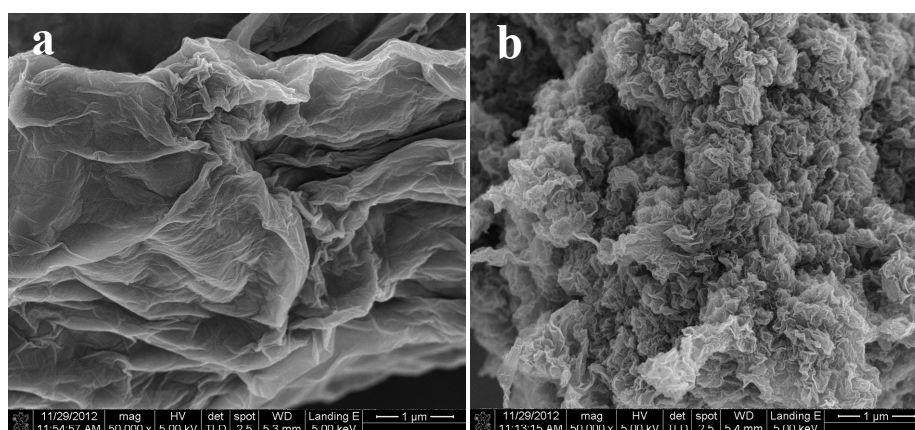


Figure 1. SEM images of (a) graphene oxide (GO) and (b) reduced graphene oxide (RGO).

In order to realize the surface functional group information of GO and RGO, the XPS spectra of the samples were analysed and are shown in Figure 2. The C1s XPS spectra of GO was decomposed to five peaks of C=C/C-C (284.4 eV), C-OH (285.7 eV), C-O-C (286.7 eV), C=O and COOH (288 and 289.1 eV) [27]. After the GO was reduced, the deconvolution of the C1s peak (RGO) showed distinguishably only a main sp^2 C=C peak and several small oxygen-bound C peaks. After a comparison, it was found that the reduction process resulted in the peak intensity of the oxygen functional groups becoming distinctly weakened. This confirmed that GO contained more O-containing functional groups than RGO.

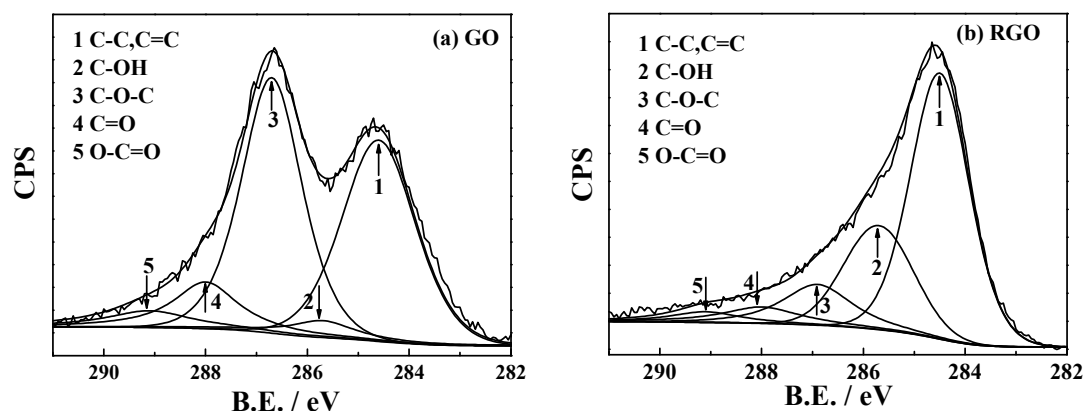


Figure 2. Deconvolution of the C1s peak of (a) GO and (b) RGO.

Figure S1 compares the FT-IR and Raman spectra of GO and RGO samples. The FT-IR spectra for GO exhibited the peaks of O-H and/or water molecule vibration (3412 cm^{-1}), C=O (COOH) stretching vibration (1726 cm^{-1}), C=C (C-C) stretching vibration (1605 cm^{-1}), O-H deformation vibration (1400 cm^{-1}), C-O (epoxy, 1221 cm^{-1}) and C-O (alkoxy, 1054 cm^{-1}) stretching vibration, respectively [28,29]. After reduction treatment, the peaks decreased significantly or even disappeared in intensity, further suggesting the removal of oxygen functional groups. In the Raman spectrum, both GO and RGO samples displayed two characteristic peaks at around 1350 and 1603 cm^{-1} , corresponding to D band and G band, respectively [29,30]. A more meticulous comparison found that the I_D/I_G value of GO (0.99) was smaller than that of RGO (1.43), probably due to a decrease in the average size of the sp^2 domains upon the reduction of GO [30].

The magnitude of the adsorption driving force of GO and RGO was studied by comparing the UV adsorption spectra of RGO (7.5 mg L^{-1}), naphthalene (1 mg L^{-1}) and their mixture in aqueous suspensions (Figure 3). The characteristic absorption occurs at 220 nm . If there is no remarkable interaction between RGO and naphthalene, the mixture absorbance should be equal to the sum of their

individual ones. However, the mixture adsorption spectrum was far below that calculated by summing the spectra of naphthalene and RGO individuals. This indicates that there is an interaction between naphthalene and RGO, which is attributed to the π - π interaction. We may estimate the strength of the π - π interaction by considering that a stronger π - π interaction will result in a greater decrease in the absorbance of the mixture at 220 nm in comparison with the sum of their individual suspensions. Therefore, it was obvious that the π - π interaction of GO for aromatics was weaker than that of RGO.

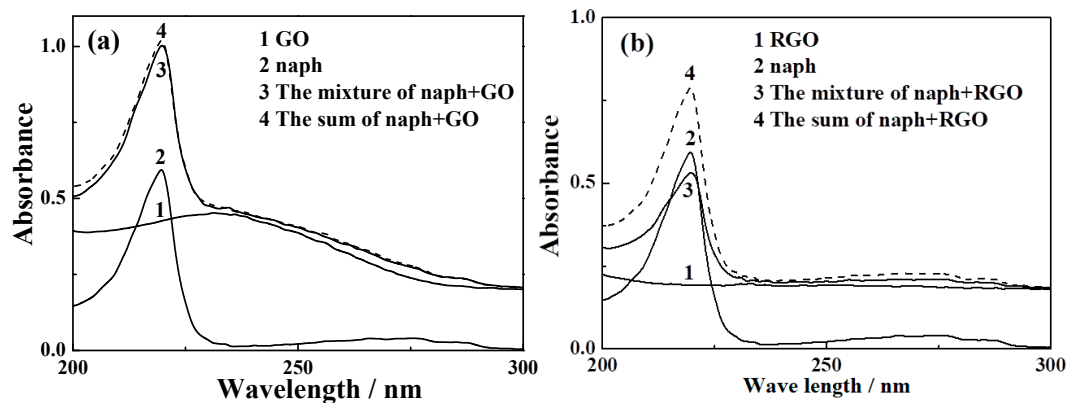


Figure 3. UV absorption spectra of the adsorbent (1), naphthalene (2) and their mixture (3). The adsorbents were (a) GO and (b) RGO. Curve 4 is the sum of (1) and (2) by calculation.

3.2. Effect of Contact Time

The effect of contact time on the adsorption of phenols (40 mg L^{-1}) on GO and RGO were investigated at pH 7 and 298 K (Figure 4). It was shown that the adsorption capacities of phenols increased quickly at the initial 20 min, and the adsorption/desorption equilibrium was reached at about 60 min. The fast adsorption was related to the structure of graphene with a single atomic layer. It was found the reduction of GO increased the values of q_e on the adsorbents (RGO > GO). The values of q_e for PE, ME, IPE, BPA and PPE on a given adsorbent were remarkably distinguished from each other, which increased from 0.271, 0.356, 0.454, 0.4 and 0.70 mmol g^{-1} on GO to 0.483, 0.841, 1.117, 1.56 and 2.054 mmol g^{-1} on RGO, respectively. Table 1 presents the existent adsorption capacity of PE and BPA in the presence of different adsorbents [31–36]. From Table 1, it was observed that RGO for the adsorption of PE and BPA had a relatively large adsorption capacity among the adsorbents.

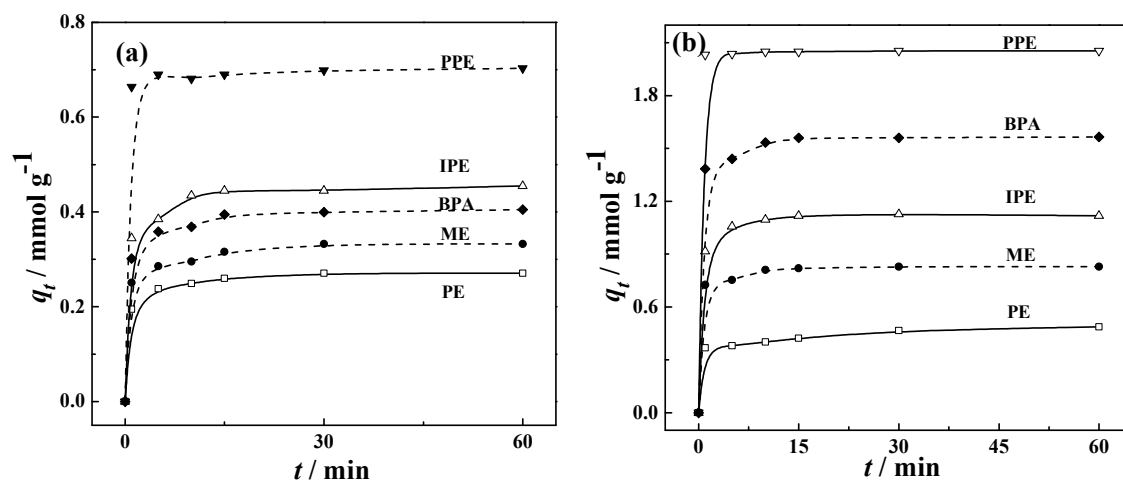


Figure 4. Effect of contact time for the adsorption of six phenols on (a) GO and (b) RGO.

Table 1. Adsorption capacity of phenol (PE) and bisphenol A (BPA) in the different systems.

Adsorbent	Phenolic Initial Concentration (mg L ⁻¹)	Adsorption Capacity (mg g ⁻¹)	Reference
GO/RGO	40 (PE)	25/45	Our work
GO/RGO	40 (BPA)	91/355	Our work
surfactant-modified zeolite	100 (BPA)	60	[31]
β -Cyclodextrin hydroxypropyl methylcellulose hydrogels	99.54 (BPA)	8	[32]
CTAB-modified graphite	300 (BPA)	125	[33]
Thermal modified activated carbon	1000 (PE)	90	[34]
zeolite X/activated carbon	103 (PE)	14	[35]
biochar	50 (PE)	28	[36]

To investigate the mechanism of the adsorption process, two conventional kinetic models (pseudo-first-order and pseudo-second-order) were applied to analyze the experimental data (see Supplementary Materials for more details). The kinetic parameters and correlation coefficients are summarized in Table S1. It was found that the kinetic data were fitted well by the pseudo-second-order model for all the five tested phenolics. Furthermore, the experimental adsorption capacity ($q_{e,exp}$) was also in accordance with the calculated adsorption capacity ($q_{e,cal}$) obtained from the pseudo-second-order model. These results indicated that the pseudo-second-order kinetic model fit the adsorption of BPA on graphene better than the pseudo-first-order model.

3.3. Effect of pH on Adsorption

The effect of pH on the adsorption of ME and BPA (40 mg L⁻¹) is presented in Figure 5. All the tested phenols have similar values of pK_a (9.8 ± 0.4 , Table S2). It was found that q_e was almost independent from the pH within the value range from 3 to pK_a , but significantly decreased when $pH > pK_a$. The phenomena were explained by the change of adsorption force. When $pH < pK_a$, the π - π stacking between phenols and graphene was the main force and pH was not the major parameter influencing the π - π interaction. When $pH > pK_a$, phenols dissociate and form negatively charged anions. Meanwhile, we monitored the zeta potentials of the adsorbents in aqueous dispersion as a function of pH (Figure S2), and found that all the samples had negative zeta potentials at pH values ranging from 5 to 11. That means that the surface of samples had a negative charge. Therefore, the electrostatic repulsion force was the main force at the range of $pH > pK_a$ and against the π - π interaction to influence the adsorption for phenols.

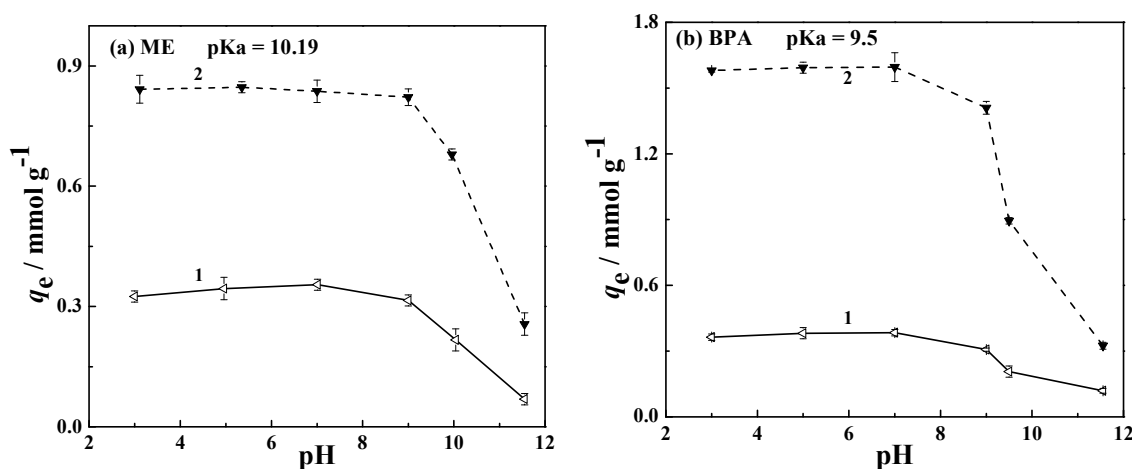


Figure 5. Variations of adsorption capacity of (a) ME and (b) BPA on (1) GO and (2) RGO as a function of pH.

3.4. Adsorption Isotherms and Thermodynamics

The adsorption isotherms of PE, ME, IPE, BPA and PPE on GO and RGO samples were measured (Figure 6), which were well estimated with the Freundlich adsorption model:

$$\ln q_e = (1/n) \ln c_e + \ln Q_F \quad (2)$$

where q_e (mmol g^{-1}) is the equilibrium adsorption capacity of the adsorbent, c_e (mmol L^{-1}) is the equilibrium concentration of adsorbate, and Q_F and n are the model constants on behalf of the adsorption capacity and the adsorption intensity, respectively. K_m ($K_m = Q_F^n$) is the median binding affinity. The related parameters fitted from the Freundlich model are listed in Table 2. It was found that for all the tested phenols, the adsorption capacity on RGO was more than that on GO. Therefore, the reduction of GO was of benefit to the adsorption of phenols. For closer comparison, a significant difference regarding the adsorption capacities of phenols with different chemical structures and solubility properties from each other was observed and increased in the order of PE < ME < IPE < BPA < PPE, which will be discussed later. The adsorption isotherms were also fitted with the Langmuir model [37]. The result showed that at the test concentration range, the Langmuir adsorption model fit the adsorption of phenols no better than the Freundlich model. The order of the adsorption capacities of phenols was similar to the Freundlich model (Table S3).

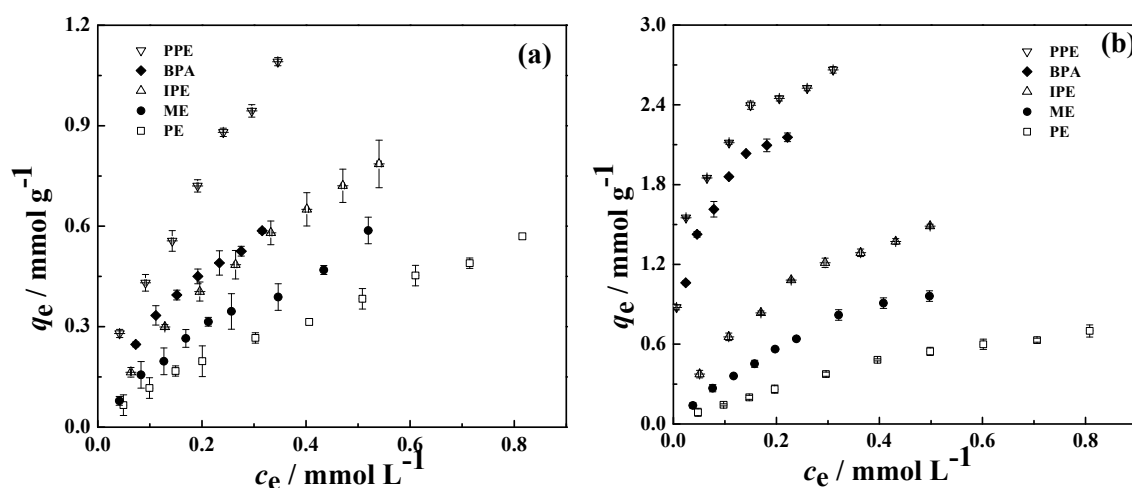


Figure 6. Adsorption isotherms of phenols on GO and RGO samples at 298K. (a) GO and (b) RGO.

Table 2. Parameters for adsorption of phenols on GO and RGO obtained by data fitting with the Freundlich model at 298 K.

Phenols	Adsorbents	Q_F ($\text{mmol}^{1-1/n} \text{L}^{1/n} \text{g}^{-1}$)	$1/n$	K_m ($\text{mmol}^{n-1} \text{L g}^{-n}$)	R^2
Phenol (PE)	GO	0.645	0.745	0.555	0.997
	RGO	0.882	0.758	0.847	0.992
4-methylphenol (ME)	GO	0.939	0.751	0.92	0.986
	RGO	1.695	0.703	2.118	0.993
4-isopropylphenol (IPE)	GO	1.264	0.723	1.382	0.995
	RGO	2.393	0.599	4.292	0.981
Bisphenol A (BPA)	GO	1.124	0.566	1.229	0.992
	RGO	3.675	0.321	57.667	0.973
2-phenylphenol (PPE)	GO	2.194	0.667	3.248	0.99
	RGO	3.819	0.272	137.89	0.968

The effect of temperature on the adsorption of phenols on GO and RGO were investigated, including 298, 313 and 333 K, from which we could obtain Q_F and K_m (Figure 7 and Table S4). The results showed that for all the tested phenols, the adsorption capacities were higher at relatively low temperatures, suggesting that a low temperature was good for adsorption.

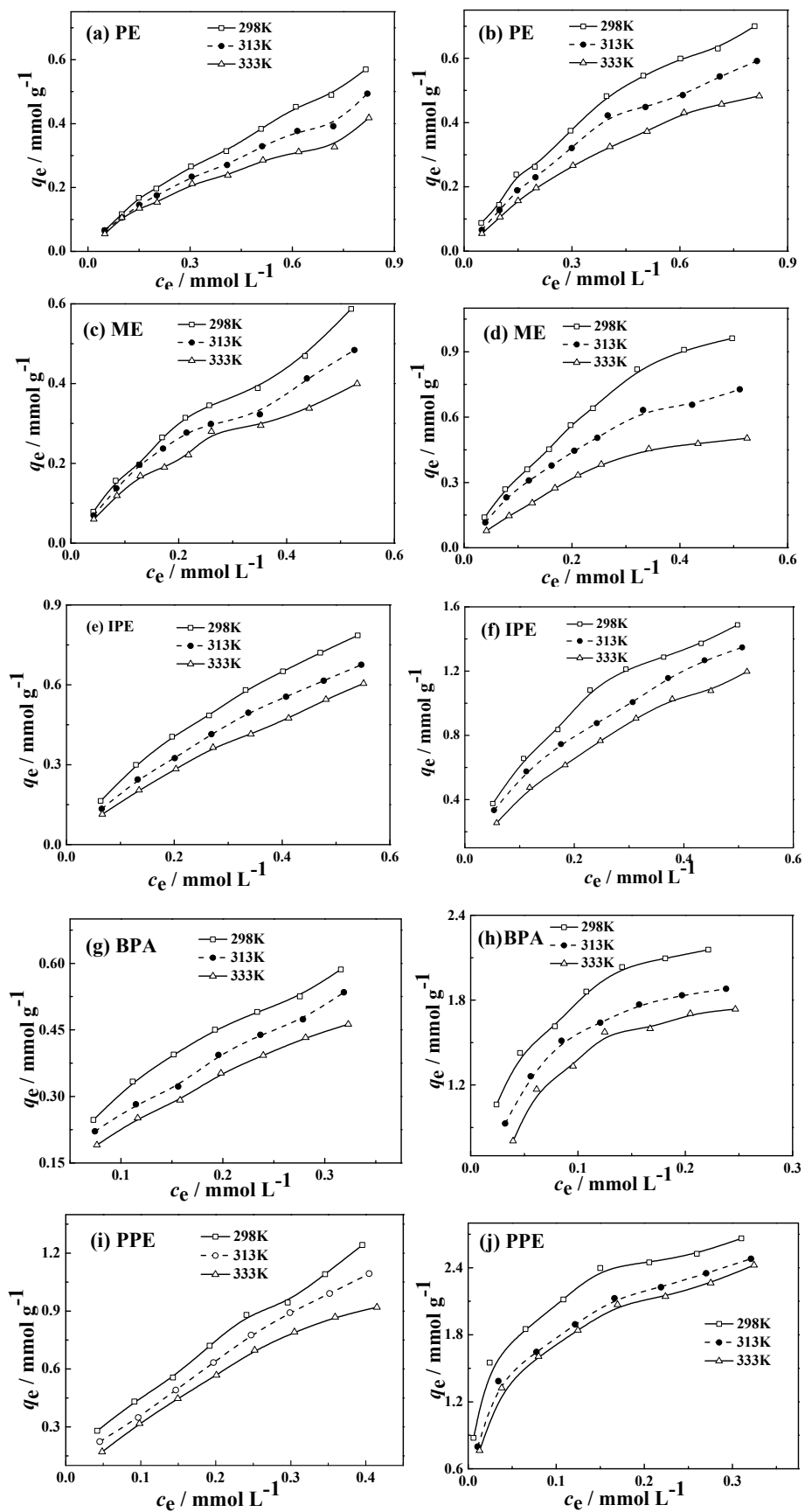


Figure 7. Adsorption isotherms of phenolics on GO (a,c,e,g,i) and RGO (b,d,f,h,j) at different temperatures.

The thermodynamic parameters ΔG^0 , ΔH^0 and ΔS^0 calculated from Equations (S1) and (S2) at three different temperatures are listed in Table 3. The negative values of ΔG^0 at three tested temperatures for all the five phenols revealed that the adsorption was a spontaneous process. Furthermore, a more negative ΔG^0 at lower temperatures meant a greater driving force to facilitate the adsorption. If performed carefully, it could be found that the values of ΔG^0 were generally low, falling in between -0.12 and -10.31 kJ mol⁻¹. This was enough to show that the adsorption was a physisorption process with a major π - π interaction. The negative ΔH^0 value suggested the exothermic nature of adsorption. The negative values of ΔS^0 indicated decreased randomness at the adsorbent/solution interface.

Table 3. Thermodynamic parameters of phenolics adsorbed on GO and RGO.

Adsorbents	Phenolics	ΔG^0 (kJ/mol)			ΔS^0 (J/mol)	ΔH^0 (kJ/mol)
		298 K	313 K	333 K		
RGO	PE	-1.37	-0.88	-0.39	-27.33	-9.48
	ME	-3.42	-3.28	-2.55	-24.32	-10.74
	IPE	-4.99	-4.73	-4.20	-21.77	-11.50
	BPA	-9.33	-9.00	-8.87	-12.21	-12.92
	PPE	-10.57	-10.04	-10.31	-6.76	-12.44
GO	PE	-0.51	-0.34	-0.12	-10.92	-3.76
	ME	-1.63	-1.47	-1.11	-14.38	-5.93
	IPE	-2.43	-1.91	-1.51	-25.68	-10.03
	BPA	-3.39	-3.01	-2.82	-15.91	-8.09
	PPE	-4.37	-3.876	-3.583	-21.786	-10.8

3.5. Effect of GO Reduction on Adsorption

Compared with the adsorption capacity of PE, ME, IPE, BPA and PPE on GO and RGO, it turned out that the q_e values of each phenol on RGO was higher than that on GO (Figure 4). To reveal the adsorption mechanisms of five adsorbates on GO and RGO, we selected naphthalene as a probe to estimate the strength of the π - π interaction of GO and RGO. It was unambiguous that the π - π interaction of GO was weaker than that of RGO (Figure 3). The reason was that surface oxygenic groups might draw and delocalize π -electrons from the basal plane of GO, inhibiting the π - π interaction between the phenols' aromatic rings and the π orbital on GO [38]. The surface oxygenic groups sharp decreased by the reduction of GO, resulting in the enhancement of the π - π interaction. Therefore, it was observed that the reduction-induced stronger π - π interaction was more favorable to the adsorption of phenols.

3.6. Effect of the Chemical Structure of Phenols on Adsorption

It was also noted that the five phenols might be divided into two groups. The first group included PE, ME and IPE, which have only one benzene ring in their molecules. The second group included BPA and PPE, which have two benzene rings in their molecules. For the first group of phenols including PE, ME and IPE, the q_e value of IPE was greater than that of ME and that of PE (Figure 4). In other words, on the two tested adsorbents, the q_e values of the first group of phenols decreased in the order of IPE > ME > PE. For the second group of phenols, the q_e values decreased in the order of PPE > BPA on the two tested adsorbents. Moreover, the q_e values of the first group of phenols were generally less than that of the second group of phenols. To account for the observations, we may consider the following aspects. (1) The increased number of benzene rings in the molecules of the phenols was favorable to the π - π interaction between the phenolic molecules and the RGO surface and hence to the adsorption of the phenolic compound. Therefore, the q_e values of the second group of phenols were generally more than that of the first group of phenols. (2) The increased steric hindrance of the substitution groups on the benzene ring was unfavorable to the π - π interaction between the phenolic

molecules and the RGO surface. Among the second group, there was a connector ($-\text{C}(\text{CH}_3)_2-$) between the two benzene rings in BPA, but no connector in PPE. The steric hindrance of the connector can account for the poorer adsorption of BPA than PPE. Among the first group of phenols, the group at the para-position on the basic phenol structure was $-\text{H}$, $-\text{CH}_3$, and $-\text{CH}(\text{CH}_3)_2$ for PE, ME and IPE, respectively. The steric hindrance of the substitution groups increased in the order of $-\text{H} < -\text{CH}_3 < -\text{CH}(\text{CH}_3)_2$, which suggested that the adsorption capacity of the phenolic compound on RGO should increase in the order of $\text{IPE} < \text{ME} < \text{PE}$. This order was reversed to the observed order of $\text{IPE} > \text{ME} > \text{PE}$ in q_e values. Consequently, the steric hindrance of the substitution groups on the benzene ring was not the major parameter influencing the π - π interaction between the first-group phenolic molecules and the RGO surface in the tested cases. (3) An electron donor will increase the electron density of the benzene ring, strengthening the π - π interaction. The order of the electron donating ability of substituent group was $-\text{H} < -\text{CH}_3 < -\text{CH}(\text{CH}_3)_2$, which was consistent with the observed order of $\text{IPE} > \text{ME} > \text{PE}$ in q_e values.

To further verify the above viewpoints, the electron distribution of target molecules was calculated using the Gaussian09 software package. The optimization of the molecular structures were performed by means of density functional theory (DFT) with Becke's three parameters and Lee–Yang–Parr's nonlocal correlation functional (B3LYP). The basis sets for C, O and H were 6–31+G (d). Figure S4 shows the π -electron density of phenols. It was found that the total electrons on phenols were, in order, $\text{PE} (-0.78 \text{ e}) < \text{ME} (-0.804 \text{ e}) < \text{IPE} (-0.82 \text{ e}) < \text{BPA} (-1.606 \text{ e}) < \text{PPE} (-2.072 \text{ e})$. The adsorption capacity of phenols on GO and RGO was plotted against the π -electron density of phenols in Figure 8. As shown from the results, in general, a positive correlation was observed. Undoubtedly, an increase in π -electron density facilitated the adsorption of phenols for GO and RGO.

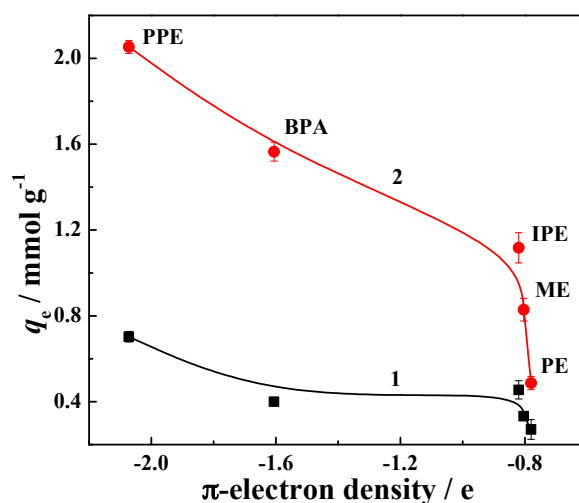


Figure 8. Adsorption capacities ($c_0 = 40 \text{ mg L}^{-1}$, $\text{pH} = 7$, $T = 298 \text{ K}$) for phenolic compounds on (1) GO and (2) RGO plotted against the π -electron density of the benzene ring of phenols.

4. Conclusions

RGO was prepared by the chemical reduction of GO, and most of the surface oxygenic groups of GO were successfully removed. A naphthalene probe method indicated that the reduction of GO could strengthen the π - π interaction. The influences of various parameters were investigated on the adsorption of PE, ME, IPE, BPA and PPE on the obtained GO and RGO. The results showed that the adsorption isotherms obeyed the Freundlich model. In addition, the adsorption efficiency of RGO for phenol removal was superior to GO. The thermodynamic analysis for the adsorption of phenols demonstrated that the adsorption process was a spontaneous, exothermic and entropy-decreasing process. The chemical structure of phenols also influenced the adsorption efficiency. It was revealed that the benzene ring numbers and the substitution groups on the benzene ring (with electron-donating

ability and stereo hindrance) influence the π - π interactions between the phenolic molecule and the RGO surface. The electron distribution of the target molecules was calculated to verify the viewpoints. Under the optimal conditions, the adsorption capacities towards PE, ME, IPE, BPA and PPE were increased from 0.271, 0.356, 0.454, 0.4 and 0.70 mmol g⁻¹ on GO to 0.483, 0.841, 1.117, 1.56 and 2.054 mmol g⁻¹ on RGO, respectively. These results will contribute to the understanding of the sorption behavior of organic pollutants on graphene.

Supplementary Materials: The following are available online at <http://www.mdpi.com/2076-3417/8/10/1950/s1>. Preparation of GO dispersion, the calculation of thermodynamic parameters, FT-IR and Raman spectra and zeta potential of GO and RGO samples, parameters of the Freundlich model at three different temperatures, thermodynamic parameters of phenolics, electron distribution of phenolics.

Author Contributions: X.W. designed and performed experiments and wrote the manuscript. Y.H., J.M. and S.L. performed the experiments. X.D. provided technical assistance with sample preparation. X.Z. and S.Y. co-designed the experiments and co-wrote the manuscript.

Acknowledgments: This work was supported by the National Natural Science Foundation of China (51372077), the Innovation and Entrepreneurship project of college students of Hubei province (201710920040), the Project of Hubei provincial department of education (Q20164503), the Natural Science Foundation of Hubei province (2017CFB140) and Shenzhen Creator Project Fundation (CKCY20170428142646043).

Conflicts of Interest: The authors declare there is no conflict of interest regarding the publication of this paper.

References

1. Liu, Q.S.; Zheng, T.; Wang, P.; Jiang, J.P.; Li, N. Adsorption isotherm, kinetic and mechanism studies of some substituted phenols on activated carbon fibers. *Chem. Eng. J.* **2010**, *157*, 348–356. [[CrossRef](#)]
2. Acikgoz, E.; Ozcan, B. Phenol biodegradation by halophilic archaea. *Int. Biodeter. Biodegr.* **2016**, *107*, 140–146. [[CrossRef](#)]
3. Ma, W.W.; Han, Y.X.; Xu, C.Y.; Han, H.J.; Ma, W.C.; Zhu, H.; Li, K.; Wang, D.X. Enhanced degradation of phenolic compounds in coal gasification wastewater by a novel integration of micro-electrolysis with biological reactor (MEBR) under the micro-oxygen condition. *Bioresour. Technol.* **2018**, *251*, 303–310. [[CrossRef](#)] [[PubMed](#)]
4. Renuka, M.K.; Gayathri, V. UV/solar light induced photocatalytic degradation of phenols and dyes by Fe(PS-BBP)Cl₃. *J. Photochem. Photobiol. A Chem.* **2018**, *353*, 477–487. [[CrossRef](#)]
5. Xiao, J.D.; Xie, Y.B.; Han, Q.Z.; Cao, H.B.; Wang, Y.J.; Nawaz, F.; Duan, F. Superoxide radical-mediated photocatalytic oxidation of phenolic compounds over Ag⁺/TiO₂: Influence of electron donating and withdrawing substituents. *J. Hazard. Mater.* **2016**, *304*, 126–133. [[CrossRef](#)] [[PubMed](#)]
6. Li, H.C.; Shan, C.; Pan, B.C. Fe(III)-doped g-C₃N₄ mediated peroxymonosulfate activation for selective degradation of phenolic compounds via high-valent iron-oxo species. *Environ. Sci. Technol.* **2018**, *52*, 2197–2205. [[CrossRef](#)] [[PubMed](#)]
7. Ai, Z.H.; Gao, Z.T.; Zhang, L.Z.; He, W.W.; Yin, J.J. Core-shell Structure dependent reactivity of Fe@Fe₂O₃ nanowires on aerobic degradation of 4-chlorophenol. *Environ. Sci. Technol.* **2013**, *47*, 5344–5352. [[CrossRef](#)] [[PubMed](#)]
8. Capocelli, M.; Prisciandaro, M.; Lancia, A.; Musmarra, D. Hydrodynamic cavitation of p-nitrophenol: A theoretical and experimental insight. *Chem. Eng. J.* **2014**, *254*, 1–8. [[CrossRef](#)]
9. Bagal, M.V.; Gogate, P.R. Degradation of 2,4-dinitrophenol using a combination of hydrodynamic cavitation, chemical and advanced oxidation processes. *Ultrason. Sonochem.* **2013**, *20*, 1226–1235. [[CrossRef](#)] [[PubMed](#)]
10. Carvajal-Bernal, A.M.; Gómez-Granados, F.; Giraldo, L.; Moreno-Piraján, J.C. A study of the interactions of activated carbon-phenol in aqueous solution using the determination of immersion enthalpy. *Appl. Sci.* **2018**, *8*, 843. [[CrossRef](#)]
11. Sanchez-Montero, M.J.; Pelaz, J.; Martin-Sanchez, N.; Izquierdo, C.; Salvador, F. Supercritical regeneration of an activated carbon fiber exhausted with phenol. *Appl. Sci.* **2018**, *8*, 81. [[CrossRef](#)]
12. Yangui, A.; Abderrabba, M.; Sayari, A. Amine-modified mesoporous silica for quantitative adsorption and release of hydroxytyrosol and other phenolic compounds from olive mill wastewater. *J. Taiwan Inst. Chem. Eng.* **2017**, *70*, 111–118. [[CrossRef](#)]

13. Xu, J.; Wang, L.; Zhu, Y.F. Decontamination of bisphenol A from aqueous solution by graphene adsorption. *Langmuir* **2012**, *28*, 8418–8425. [[CrossRef](#)] [[PubMed](#)]
14. Morozov, S.V.; Novoselov, K.S.; Schedin, F.; Jiang, D.; Firsov, A.A.; Geim, A.K. Two-dimensional electron and hole gases at the surface of graphite. *Phys. Rev. B* **2005**, *72*, 201401. [[CrossRef](#)]
15. Zhou, Y.; Apul, O.G.; Karanfil, T. Adsorption of halogenated aliphatic contaminants by graphene nanomaterials. *Water Res.* **2015**, *79*, 57–67. [[CrossRef](#)] [[PubMed](#)]
16. Majidi, R.; Karami, A.R. Caffeine and nicotine adsorption on perfect, defective and porous graphene sheets. *Diam. Relat. Mater.* **2016**, *66*, 47–51. [[CrossRef](#)]
17. Xu, J.; Cao, Z.; Zhang, Y.L.; Yuan, Z.L.; Lou, Z.M.; Xu, X.H.; Wang, X.K. A review of functionalized carbon nanotubes and graphene for heavy metal adsorption from water: Preparation, application, and mechanism. *Chemosphere* **2018**, *195*, 351–364. [[CrossRef](#)] [[PubMed](#)]
18. Yang, X.Z.; Shi, Z.; Yuan, M.Y.; Liu, L.S. Adsorption of trivalent antimony from aqueous solution using graphene oxide: Kinetic and thermodynamic studies. *J. Chem. Eng. Data* **2015**, *60*, 806–813. [[CrossRef](#)]
19. Ramesha, G.K.; Kumara, A.V.; Muralidhara, H.B.; Sampath, S. Graphene and graphene oxide as effective adsorbents toward anionic and cationic dyes. *J. Colloid Interface Sci.* **2011**, *361*, 270–277. [[CrossRef](#)] [[PubMed](#)]
20. Mu'azu, N.D.; Jarrah, N.; Zubair, M.; Alagha, O. Removal of phenolic compounds from water using sewage sludge-based activated carbon adsorption: A review. *Int. J. Environ. Res. Public Health* **2017**, *14*, 1094. [[CrossRef](#)] [[PubMed](#)]
21. Erto, A.; Chianese, S.; Lancia, A.; Musmarra, D. On the mechanism of benzene and toluene adsorption in single-compound and binary systems: Energetic interactions and competitive effects. *Desalin. Water Treat.* **2017**, *86*, 259–265. [[CrossRef](#)]
22. Björk, J.; Hanke, F.; Palma, C.A.; Samori, P.; Cecchini, M.; Persson, M. Adsorption of aromatic and anti-aromatic systems on graphene through π - π Stacking. *J. Phys. Chem. Lett.* **2010**, *1*, 3407–3412. [[CrossRef](#)]
23. Zhao, G.X.; Jiang, L.; He, Y.D.; Li, J.X.; Dong, H.L.; Wang, X.K.; Hu, W.P. Sulfonated Graphene for Persistent Aromatic Pollutant Management. *Adv. Mater.* **2011**, *23*, 3959–3963. [[CrossRef](#)] [[PubMed](#)]
24. Lee, J.; Min, K.A.; Hong, S.; Kim, G. Ab initio study of adsorption properties of hazardous organic molecules on graphene: Phenol, phenyl azide, and phenylnitrene. *Chem. Phys. Lett.* **2015**, *618*, 57–62. [[CrossRef](#)]
25. He, L.; Liu, F.F.; Zhao, M.Y.; Qi, Z.; Sun, X.F.; Afzal, M.Z.; Sun, X.M.; Li, Y.H.; Hao, J.C.; Wang, S.G. Electronic-property dependent interactions between tetracycline and graphene nanomaterials in aqueous solution. *J. Environ. Sci.* **2018**, *66*, 286–294. [[CrossRef](#)] [[PubMed](#)]
26. Chen, X.X.; Chen, B.L. Macroscopic and spectroscopic investigations of the adsorption of nitroaromatic compounds on graphene oxide, reduced graphene oxide, and graphene nanosheets. *Environ. Sci. Technol.* **2015**, *49*, 6181–6189. [[CrossRef](#)] [[PubMed](#)]
27. Ren, P.G.; Yan, D.X.; Ji, X.; Chen, T.; Li, Z.M. Temperature dependence of graphene oxide reduced by hydrazine hydrate. *Nanotechnology* **2011**, *22*, 055705. [[CrossRef](#)] [[PubMed](#)]
28. Jiao, T.F.; Guo, H.Y.; Zhang, Q.R.; Peng, Q.M.; Tang, Y.F.; Yan, X.H.; Li, B.B. Reduced graphene oxide-based silver nanoparticle-containing composite hydrogel as highly efficient dye catalysts for wastewater treatment. *Sci. Rep.* **2015**, *5*, 11873. [[CrossRef](#)] [[PubMed](#)]
29. Wang, X.B.; Tang, H.Q.; Huang, S.S.; Zhu, L.H. Fast and facile microwave-assisted synthesis of graphene oxide nanosheets. *RSC Adv.* **2014**, *4*, 60102–60105. [[CrossRef](#)]
30. Stankovich, S.; Dikin, D.A.; Piner, R.D.; Kohlhaas, K.A.; Kleinhammes, A.; Jia, Y.Y.; Wu, Y.; Nguyen, S.T.; Ruoff, R.S. Synthesis of graphene-based nanosheets via chemical reduction of exfoliated graphite oxide. *Carbon* **2007**, *45*, 1558–1565. [[CrossRef](#)]
31. Dong, Y.; Wu, D.; Chen, X.; Lin, Y. Adsorption of bisphenol A from water by surfactant-modified zeolite. *J. Colloid Interface Sci.* **2010**, *348*, 585–590. [[CrossRef](#)] [[PubMed](#)]
32. De Souza, Í.F.T.; Petri, D.F.S. β -Cyclodextrin hydroxypropyl methylcellulose hydrogels for bisphenol A adsorption. *J. Mol. Liq.* **2018**, *266*, 640–648. [[CrossRef](#)]
33. Wang, L.C.; Ni, X.J.; Cao, Y.H.; Cao, G.Q. Adsorption behavior of bisphenol A on CTAB-modified graphite. *Appl. Surf. Sci.* **2018**, *428*, 165–170. [[CrossRef](#)]
34. Zhang, D.F.; Huo, P.L.; Liu, W. Behavior of phenol adsorption on thermal modified activated carbon. *Chin. J. Chem. Eng.* **2016**, *24*, 446–452. [[CrossRef](#)]
35. Cheng, W.P.; Gao, W.; Cui, X.Y.; Ma, J.H.; Li, R.F. Phenol adsorption equilibrium and kinetics on zeolite X/activated carbon composite. *J. Taiwan Inst. Chem. Eng.* **2016**, *62*, 192–198. [[CrossRef](#)]

36. Mohammed, N.A.S.; Abu-Zurayk, R.A.; Hamadneh, I.; Al-Dujaili, A.H. Phenol adsorption on biochar prepared from the pine fruit shells: Equilibrium, kinetic and thermodynamics studies. *J. Environ. Manag.* **2018**, *226*, 377–385. [[CrossRef](#)] [[PubMed](#)]
37. Nielsen, L.; Biggs, M.J.; Skinner, W.; Bandosz, T.J. The effects of activated carbon surface features on the reactive adsorption of carbamazepine and sulfamethoxazole. *Carbon* **2014**, *80*, 419. [[CrossRef](#)]
38. Pei, Z.G.; Li, L.Y.; Sun, L.X.; Zhang, S.Z.; Shan, X.Q.; Yang, S.; Wen, B. Adsorption characteristics of 1,2,4-trichlorobenzene, 2,4,6-trichlorophenol, 2-naphthol and naphthalene on graphene and graphene oxide. *Carbon* **2013**, *51*, 156–163. [[CrossRef](#)]



© 2018 by the authors. Licensee MDPI, Basel, Switzerland. This article is an open access article distributed under the terms and conditions of the Creative Commons Attribution (CC BY) license (<http://creativecommons.org/licenses/by/4.0/>).